

Received August 28, 2019, accepted September 9, 2019, date of publication September 19, 2019, date of current version October 2, 2019.

Digital Object Identifier 10.1109/ACCESS.2019.2942363

Design and Optimization of Nonuniform Helical Antennas With Linearly Varying Geometrical Parameters

JELENA DINKIĆ¹, DRAGAN OLČAN¹, (Member, IEEE), ANTONIJE DJORDJEVIĆ^{1,2}, AND ALENKA ZAJIĆ³, (Senior Member, IEEE)

¹School of Electrical Engineering, University of Belgrade, 11120 Belgrade, Serbia

²Serbian Academy of Sciences and Arts, 11000 Belgrade, Serbia

³School of Electrical and Computer Engineering, Georgia Institute of Technology, Atlanta, GA 30332, USA

Corresponding author: Alenka Zajić (alenka.zajic@ece.gatech.edu)

This work was supported in part by the DARPA LADS under Contract FA8650-16-C-7620.

ABSTRACT Nonuniform helical antennas have many degrees of freedom, which makes the search space for the optimal design very challenging. The objective of this paper is to systematically analyze nonuniform helical antennas with linearly varying geometrical parameters and to provide analytical equations that approximate the optimal design and the gain of the designed antennas. Using various optimization algorithms, we made a large database of the optimal nonuniform helical antennas with linearly varying geometrical parameters. Based on these results, we made analytical equations that approximate the optimal design and the gain of the designed antennas. These equations allow for a fast design procedure yielding all necessary parameters needed for the design and fabrication of nonuniform helical antennas that meet specified characteristics. Special attention is devoted to antenna losses. Antennas designed following the presented procedure achieve around 2.5 dB higher gain than uniform helical antennas of the same axial length, while maintaining the bandwidth and axial ratio. As a verification of the proposed design procedure, a helical antenna with the central operating frequency of 1 GHz was designed, simulated, fabricated, and measured. The comparison between measured and simulated results confirms the validity of the presented design procedure.

INDEX TERMS Nonuniform helical antennas, optimization.

I. INTRODUCTION

Since the first report by Kraus in [1], helical antennas have been widely used due to a simple structure, almost circular polarization in the axial radiating mode, inherently broad bandwidth, etc. Practical guidelines are available for design of uniform helical antennas [1]–[7]. In [7], a reliable design procedure for uniform helical antennas is presented based on systematic investigation and comparison with other guidelines. On the other hand, such guidelines do not exist for nonuniform antennas, although various properties of nonuniform antennas have been investigated. In [8], it is shown that the tapered radii at the feeding end and the termination improve the radiation properties and impedance behavior. Tapered (or conical) helices allow shaping the gain versus frequency and improve the axial ratio and radiation pattern [9].

The associate editor coordinating the review of this manuscript and approving it for publication was Wen-Sheng Zhao.

Logarithmic, linear, and exponential variations of the turn radius are presented in [10], [11], but the highest reported gain is around 6.5 dB lower than the gain of uniform helical antennas of the same axial length [7]. In [12], nonuniform helical antennas have a wire pigtail instead of a ground plane, while both the radii and pitches are optimized for the maximum gain. The resulting antennas are smaller and handier, without compromising the gain. In [13], [14], nonlinear pitch profiles are considered with a constant or exponentially varying turn radius. In [15], an exponential pitch is considered for widening the bandwidth. The design of dual-band helical antennas, working in the normal mode, is presented in [16], [17].

Nonuniform helical antennas have many degrees of freedom, which makes the optimization very challenging. Our investigation shows that nonuniform helical antennas with linearly, exponentially, and piecewise-linearly varying geometrical parameters achieve practically the same gain [18]. Furthermore, nonuniform helical antennas with

piecewise-linear variations of geometrical parameters have additional degrees of freedom, which sometimes leads to technically unacceptable results. Hence, the objective of this paper is to systematically analyze nonuniform helical antennas with linearly varying geometrical parameters, i.e., helical antennas where the radii and pitch angles of turns change linearly along the axis of the antenna.

We consider nonuniform helical antennas located above a ground plane because they achieve about 2.5 dB higher gain compared to uniform helical antennas of the same axial length. This is due to the downward radiation (the backward wave) that is reflected from the ground plane and then catches up with the upward radiation.

By having practical applications in mind, we consider the following limits:

- operating frequencies from 30 MHz to 6 GHz,
- wire conductivities from 10 MS/m to 100 MS/m,
- axial antenna lengths from 2λ to 10λ , and
- wire radii from 0.0002λ to 0.002λ ,

where λ is the wavelength at the operating frequency. These limits define a hyper rectangle, and the design procedure should be valid for as large as possible subspace within it.

We created a large database of the optimal nonuniform helical antennas, involving around 5 million antenna simulations. The obtained optimal parameters are analytically approximated, enabling a quick design for given antenna specification.

In order to verify the proposed design procedure, we have fabricated and measured a prototype helical antenna.

The authors believe that the quick and reliable design procedure presented in this paper can be useful in many applications, as, for example, for the design of reconfigurable helical antennas that have been proposed in [19]–[25].

The rest of the paper is organized as follows. Section II defines the typical geometry of the considered helical antennas. Section III presents the optimization setup. Section IV specifically addresses conductor losses. Section V summarizes the optimal antenna parameters. Section VI details the design procedure. Section VII summarizes bandwidth, axial ratio and impedance. Section VIII discusses the influence of the finite ground plane. Section IX describes the prototype used for the verification and compares properties of antennas designed following the proposed procedure with other helical antennas presented in the literature. Finally, Section X concludes the paper.

II. HELICAL ANTENNAS WITH LINEARLY VARYING GEOMETRICAL PARAMETERS AND CORRESPONDING ANTENNA MODELS

The typical geometry of a helical antenna with linearly varying geometrical parameters is shown in Fig. 1. The antenna counterbalance can be a wire pigtail [12], which is suitable for compact antennas, or the antenna can be located above an infinite ground plane (theoretical case), a finite ground plane, or reflectors of various shapes. The optimal shape and dimension of the finite ground plane and the reflector can

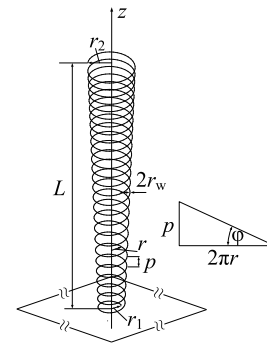


FIGURE 1. Sketch of nonuniform helical antenna.

increase the antenna gain [26]–[29]. In this paper, our investigation is mostly oriented towards the design of the helical conductor, while the ground is flat and predefined. With that objective in mind, we first consider helices located above an infinite, perfectly conducting (PEC) ground plane. Second, in Section VIII, we examine finite ground planes in order to complete the design procedure, suitable for production.

The antenna conductor can be a wire, a ribbon, or a strip [30]. Here, we consider only wire conductors, whose cross-section is circular and uniform along the antenna.

The geometry of the helical antenna is defined by the turn radius, r , the pitch, p (or the pitch angle, φ), and the overall axial antenna length, L (Fig. 1). The pitch angle is related to the turn radius and the pitch as $\varphi = \arctan(p/2\pi r)$. In the case of a nonuniform helical antenna with linearly varying geometrical parameters, the pitch angle and the radius are linear functions of the axial coordinate (z) along the antenna (i.e., linear distributions are assumed):

$$r = (r_2 - r_1)\frac{z}{L} + r_1, \quad \varphi = (\varphi_2 - \varphi_1)\frac{z}{L} + \varphi_1, \quad (1)$$

where r_1 is the radius at the bottom of the helix (i.e., for $z = 0$), r_2 is the radius at the top ($z = L$), and, similarly, φ_1 and φ_2 are the pitch angles at the bottom and top of the helix, respectively. In our design, the optimal coefficients r_1 , r_2 , φ_1 , and φ_2 are functions of the antenna axial length L , the radius of the wire conductor, r_w , and the operating frequency.

Simulations are performed in software WIPL-D [31], and the results are cross-checked in software AWAS [32]. Examples of models made in WIPL-D are shown in Fig. 2. These two programs can analyze only straight-line wire segments. To that purpose, we approximate a circular turn of radius r by a regular polygon that has n sides. We assume that the polygon is inscribed into a circle whose radius is $r_{\text{out}} = 2r/(1 + \cos(\Delta\gamma/2))$, where $\Delta\gamma = 2\pi/n$ is the central angle of the polygon. The circle of radius r is midway between the circumscribed circle and the inscribed circle of the polygon.

We have found by extensive numerical computations that for such r_{out} , the gain of the helical antennas practically does not depend on n for $n \geq 12$: the antenna gain deviates less than 0.1 dB compared to a very large n . Nonetheless,

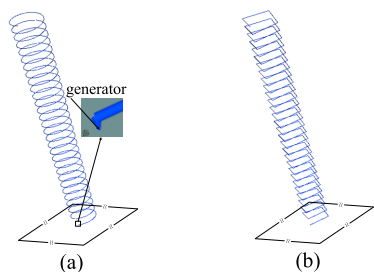


FIGURE 2. WIPL-D model of nonuniform helical antenna (a) with polygonal turns (16 sides) and (b) with square turns.

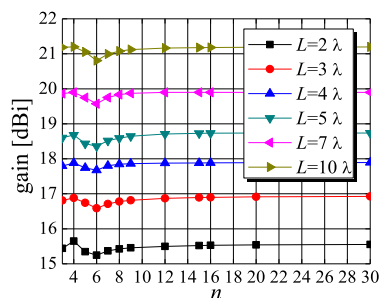


FIGURE 3. Gain of antennas for various numbers of sides of the approximating polygon (n) for helical antennas of various axial lengths (L).

the same low discrepancy was also found for $n = 4$ (i.e., for square turns), as shown in Fig. 3. Note that by controlling r_{out} the gain of a helix with circular turns can be achieved for arbitrary n .

Further, a small n is useful to speed-up computations. Finally, for $n = 4$ we can use a simple dielectric support for the wire that has an almost negligible influence on the antenna characteristics. Hence, in all computations and models presented in this paper, we use $n = 4$, knowing that almost the same gain is practically achieved with perfectly round turns.

In our models, the generator that feeds the antenna is located at the bottom of a short vertical wire segment, between the ground plane and the beginning of the first turn (Fig. 2a).

III. OPTIMIZATION SETUP

We optimized the antenna geometry in order to maximize the partial gain [33] for the circular polarization in the main radiating direction.

For various axial antenna lengths and wire radii, we optimized the radii and pitch angles of the first and the last turns. The radii and pitch angles of other turns were calculated using (1). We considered the wires to be lossy and the optimization of the antenna geometry was performed for various wire conductivities, including a PEC. An infinite ground plane was assumed, made out of a PEC.

Combinations of the optimization variables that correspond to infeasible geometries were rejected during the optimization.

Comparison of optimization algorithms that we used for the design of nonuniform helical antennas is presented

in [34]. It is shown that PSO [35], [36], with Nelder-Mead simplex [37] launched from the best found PSO solution, leads to the highest probability of finding the best solution, among all considered optimization strategies. Therefore, in this paper we have performed a two-step optimization: PSO with 2000 iterations followed by Nelder-Mead simplex with 200 iterations.

IV. MODELING OF LOSSES DUE TO FINITE CONDUCTIVITY

As stated in Section I, the range of the conductivities was chosen to cover the frequency range of operation for helical antennas that are of practical interest, from 10 MS/m (corresponding to brass) up to 100 MS/m (slightly better than silver). We scaled (normalized) the antenna dimensions and conductivities in order to perform all simulations at 300 MHz (where the wavelength is practically $\lambda = 1$ m), with the aim that the design should be applicable to antennas operating in the frequency range from 30 MHz to 6 GHz. According to the similitude theorem [38], if the operating frequency is increased s times, linear geometrical dimensions should be decreased s times and the wire conductivity should be increased s times in order to obtain electromagnetic similarity. Hence, the wire conductivities in the scaled model were taken to be in the range from 0.5 MS/m to 1000 MS/m. Optimizations were performed for sets of antenna axial lengths and wire radii within the limits defined in Section I.

Hence, it is convenient to consider the geometrical dimensions divided by the wavelength, and the conductivity multiplied by the wavelength. This normalization enables easy translation of the design to the actual wavelength.

The gain of the optimal antennas is shown in Fig. 4 by solid blue lines, for various antenna axial lengths and wire radii, as a function of the conductivity (for the scaled models). For comparison, the gain of the optimal uniform antennas is also shown by horizontal dashed red lines [7]. The conductor losses strongly affect the gain of the nonuniform antennas with linearly varying geometrical parameters, unlike the uniform helical antennas for which the effect of losses is much smaller even for the thinnest wires considered in [7].

Solid cyan lines and dots in Fig. 4 are related to the proposed design, which is explained in the following section.

The shape of the optimal nonuniform helical antennas, whose gain is shown in Fig. 4, depends on the wire conductivity, i.e., on the losses. When the losses are high (i.e., when the conductivity is low, far left from the dots in Fig. 4), the radii and pitch angles of the turns near the feeding point (at the helix bottom) are larger than the radii and pitch angles of the turns closer to the helix top, and the antenna gain is small. A typical geometry of the antenna in this case is shown in Fig. 5a. When the losses are very high, the gain of the nonuniform antennas approaches the gain of the uniform antennas. (The uniform helical antennas can be considered as a special case of the nonuniform antennas.) Hence, for the simplicity of the design and manufacturing, the uniform antennas may be the preferred engineering solution in such cases.

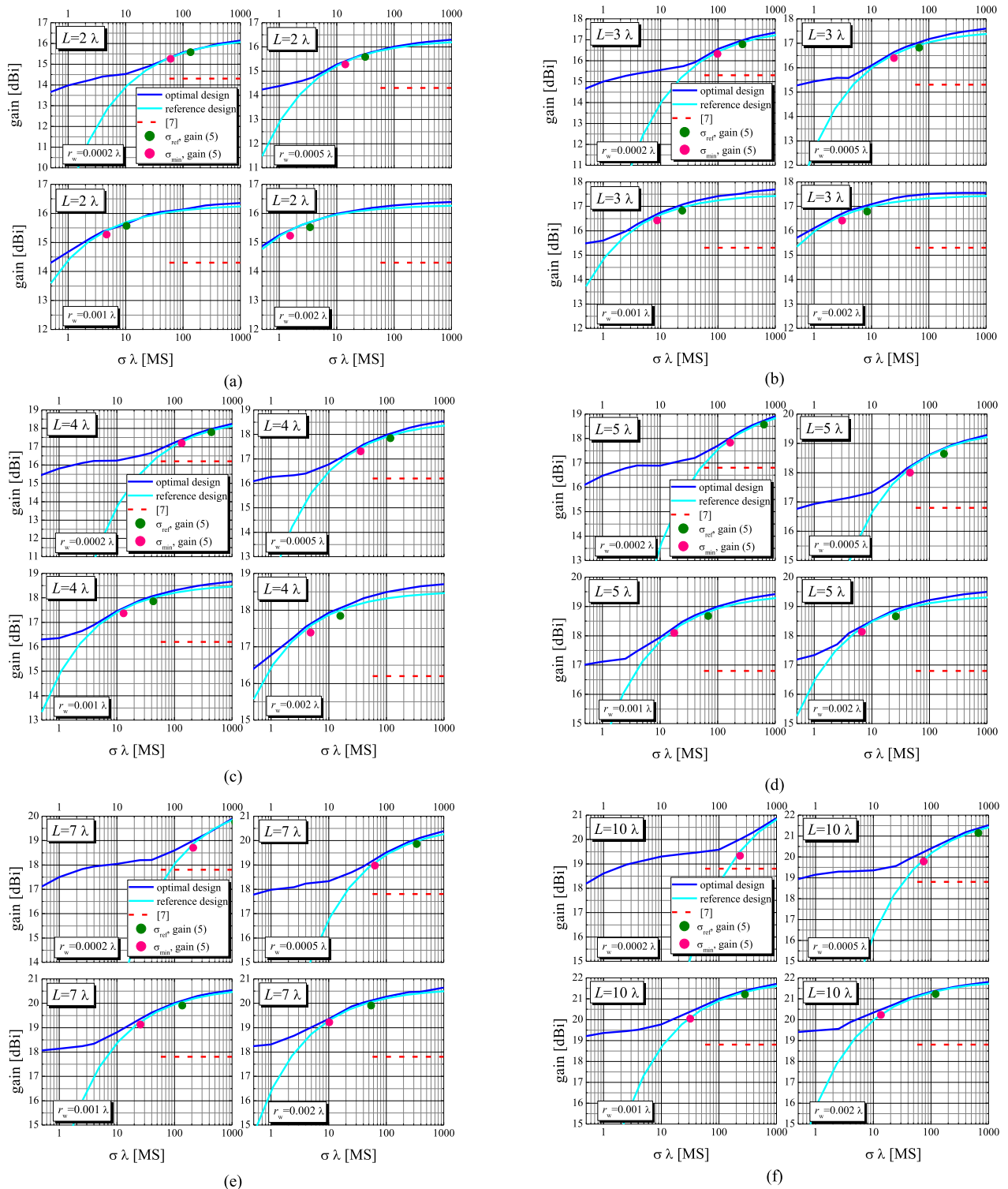


FIGURE 4. Computed gain of helical antennas versus normalized conductivity ($\sigma \lambda$) for various wire radii and axial antenna lengths (a) $L = 2 \lambda$, (b) $L = 3 \lambda$, (c) $L = 4 \lambda$, (d) $L = 5 \lambda$, (e) $L = 7 \lambda$, and (f) $L = 10 \lambda$. Solid blue lines show the gain of the optimal nonuniform antennas. Dashed red lines show the gain of the optimal uniform helical antennas from [7]. Solid cyan lines show the computed gain of antennas designed using (3), (4). Abscissas of green and pink dots correspond to the normalized conductivities evaluated using (2) and (6), respectively, and ordinates correspond to the estimated gain evaluated using (5).

As the losses diminish (i.e., as the conductivity increases), in the region around the dots in Fig. 4, the geometry smoothly changes to the geometry shown in Fig. 5b, where the radii

and pitch angles increase from the helix bottom towards the top. For simplicity, we shall refer to such losses as medium losses.

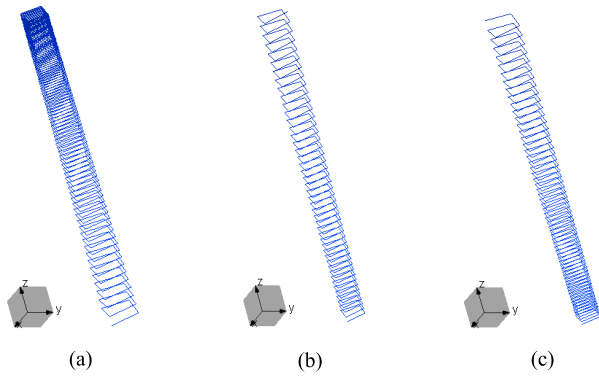


FIGURE 5. Typical examples of geometries of the optimal antennas for: (a) high losses (b) medium losses, and (c) low losses.

With further decrease of losses (i.e., increase of the conductivity, far right from the dots in Fig. 4), including PEC wires, pitch angles of the turns close to the feeding point become very small, as shown in Fig. 5c. In this region, the turns become close to each other (almost touching each other). In addition, the overall wire length becomes very long because the number of turns is large, which may be impractical.

V. OPTIMAL ANTENNA DESIGN

The objective in this section is to provide a simple, yet sufficiently accurate design procedure for nonuniformly-wound helical antennas. We performed detailed investigation of the optimal antennas for various conductivities (including PEC wires), for various antenna lengths, and wire radii. We established that it is possible to find a unique design for each axial length and wire radius that is valid in a wide range of conductivities, but does not depend on the conductivity. This reference design is obtained by optimizing the antenna at the reference conductivity σ_{ref} defined by

$$\sigma_{\text{ref}} \lambda = 10^{(0.5154 \log_{10}(\frac{r_w}{\lambda}) + 3.601) \log_{10}(\frac{L}{\lambda}) - 1.750 \log_{10}(\frac{r_w}{\lambda}) - 4.850}, \quad (2)$$

where L , r_w , and λ are in meters, and σ_{ref} is in MS/m. The shape of the reference design corresponds to the geometry shown in Fig. 5b.

The normalized reference conductivity is plotted in Fig. 6 as a function of the normalized axial length and normalized wire radius. The normalization is with respect to the wavelength. Fig. 7 shows the design parameters for the reference design.

For the reference design, we performed two-dimensional interpolation and approximated the optimal parameters by:

$$\frac{r_m}{\lambda} = \left(A_r \frac{r_w}{\lambda} + B_r \right) \log_{10} \left(\frac{L}{\lambda} \right) + \left(C_r \log_{10} \left(\frac{r_w}{\lambda} \right) + D_r \right), \quad (3)$$

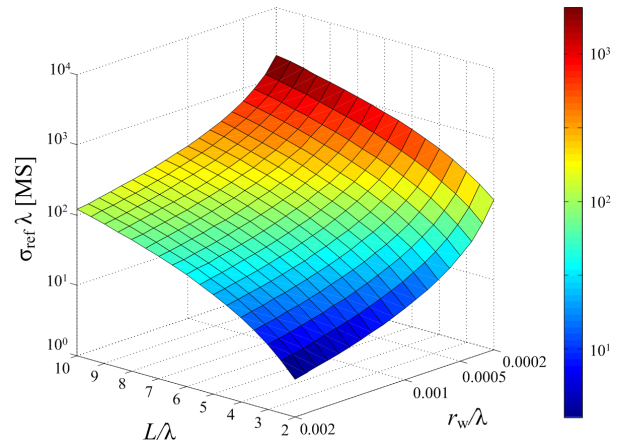


FIGURE 6. Normalized reference conductivity ($\sigma_{\text{ref}} \lambda$), as a function of the normalized antenna axial length (L/λ) and normalized wire radius (r_w/λ).

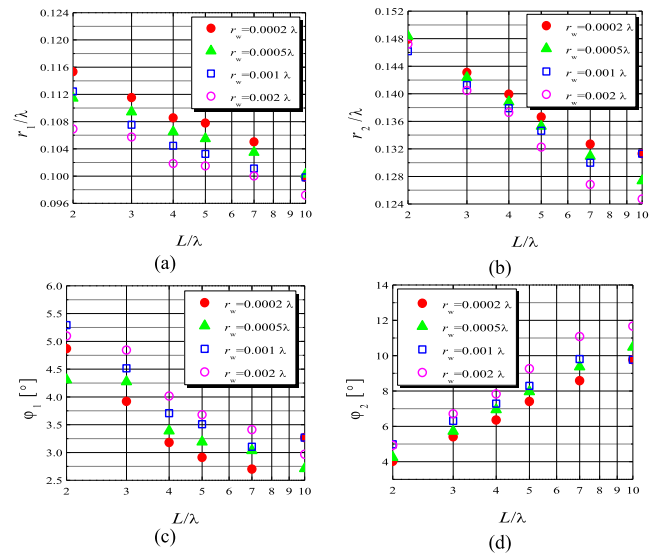


FIGURE 7. Design parameters of the reference design: (a) normalized radius of the first turn (r_1/λ), (b) normalized radius of the last turn (r_2/λ), (c) pitch angle of the first turn (ϕ_1), and (d) pitch angle of the last turn (ϕ_2), versus normalized antenna axial length (L/λ).

$m = 1, 2$, where the coefficients A_r , B_r , C_r , and D_r are listed in Table I, and

$$\begin{aligned} \phi_1 &= - \left(1.4010 \log_{10} \left(\frac{r_w}{\lambda} \right) + 7.2219 \right) \log_{10} \left(\frac{L}{\lambda} \right) \\ &\quad + \left(1.4980 \log_{10} \left(\frac{r_w}{\lambda} \right) + 10.256 \right), \\ \phi_2 &= \left(891.19 \frac{r_w}{\lambda} + 7.6254 \right) \log_{10} \left(\frac{L}{\lambda} \right) \\ &\quad + \left(0.31695 \log_{10} \left(\frac{r_w}{\lambda} \right) + 2.7238 \right), \end{aligned} \quad (4)$$

where the pitch angles are in degrees.

The coefficients in (2), (4), and Table I were obtained by heuristic investigation of various dependences in linear, logarithmic, and exponential scale, and by including fine-tuning terms. The investigation was followed by optimization

TABLE 1. Coefficients in (3).

m	A_r	B_r	C_r	D_r
1	1.0681	-0.0190	-0.00770	0.0910
2	-2.2001	-0.0250	0.00113	0.160

of the coefficients and verification by simulations of the designed antennas. Special attention was paid to differences of the gain of the optimal antennas and the antennas designed using (3), (4). That discrepancy was maintained as low as possible.

For the antennas designed using (3), (4) we also provide an approximate equation that estimates the gain:

$$\text{gain} = 8.385 \log_{10} \left(\frac{L}{\lambda} \right) + 13.48 - \frac{0.002983 \frac{L}{\lambda}}{\left(\frac{r_w}{\lambda} \right)^{0.8411} \sqrt{\sigma \lambda}} + \frac{26.89}{\left(\frac{L}{\lambda} \right)^{6.763}} - 68.71 \frac{r_w}{\lambda}, \quad (5)$$

where L , r_w , and λ are in meters, σ is in MS/m, and the gain is in dBi. The coefficients in (5) were obtained following the described procedure, but two other goals were also targeted. First, the calculated gain should deviate as little as possible from the simulated gain of the antennas designed using parameters calculated from (3) and (4). Second, (5) must underestimate the gain.

The computed gain of the antennas designed using (3), (4) is shown in Fig. 4 by solid cyan lines. Obviously, for normalized conductivities in the range $\sigma_{\text{ref}} \lambda < \sigma \lambda < 1000$ MS, i.e., from $\sigma_{\text{ref}} \lambda$ up to the highest normalized conductivity considered (1000 MS), the gain of the antennas obtained using the reference design is only up to 0.25 dB lower than the gain of the corresponding optimal antennas. Although normalized conductivities higher than 1000 MS do not correspond to any design within the hyper rectangle defined in Section I, we note that if we use the reference design (3), (4) and then assume a PEC wire, the resulting gain is up to 0.4 dB lower than the gain of the antenna optimized immediately assuming a PEC wire.

The reference design (3), (4) can also be used for normalized conductivities $\sigma \lambda < \sigma_{\text{ref}} \lambda$, as shown in Fig. 4. Even when the normalized conductivity is

$$\sigma_{\text{min}} \lambda = (0.5954 - 0.4830 \log_{10} (L/\lambda)) \sigma_{\text{ref}} \lambda, \quad (6)$$

the gain of the designed antennas (pink dots in Fig. 4) is in the worst case around 0.5 dB lower than the gain of the corresponding optimal antennas. Hence, the proposed design can be used for $\sigma_{\text{min}} \lambda < \sigma \lambda < 1000$ MS. In (6) L and λ are in meters, and σ_{min} and σ_{ref} are in MS/m. If $\sigma_{\text{min}} \lambda < \sigma \lambda < 1000$ MS, the maximal underestimate of the gain evaluated from (5) is 0.3 dB.

The abscissas of the green and pink dots shown in Fig. 4 are given by (2) and (6), respectively, whereas the ordinates are obtained from (5) for $\sigma \lambda = \sigma_{\text{ref}} \lambda$ and $\sigma \lambda = \sigma_{\text{min}} \lambda$. For the thinnest wire and axial antenna lengths 7λ and 10λ ,

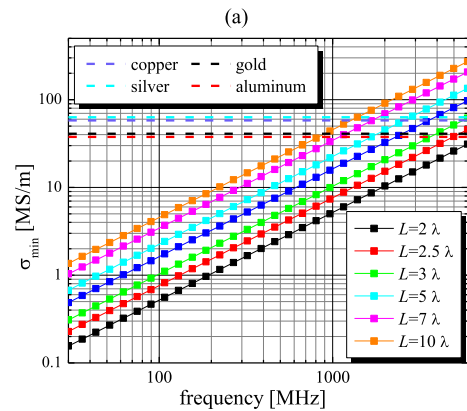
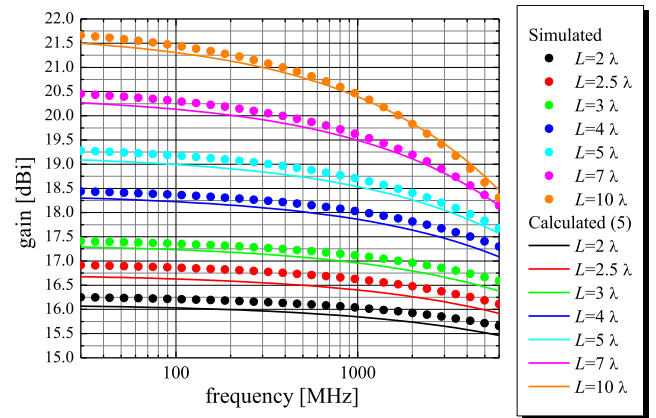


FIGURE 8. (a) Gain for $\sigma = 58$ MS/m and (b) σ_{min} for $r_w = 0.002 \lambda$ and various axial lengths in the operating frequency range defined in Section I. For reference, horizontal dashed lines show conductivities of copper, gold, silver, and aluminum.

$\sigma_{\text{ref}} \lambda > 1000$ MS. Hence in these cases only a pink dot is shown in Fig. 4.

Fig. 8 shows the gain for various axial lengths in the operating frequency range from 30 MHz to 6 GHz, as defined in Section I, and σ_{min} calculated from (6). For all antennas, the wire radius is 0.002λ and the conductivity is 58 MS/m (copper), but the results are qualitatively the same for all wire radii within the limits defined in Section I. The results shown in Fig. 8 confirm that (5) correctly predicts the gain and also satisfies the assumption that the gain is underestimated as long as the wire conductivity is higher than σ_{min} at the considered frequency.

VI. DESIGN PROCEDURE

In this section, we outline the procedure for a quick design of nonuniform helical antennas with linearly varying geometrical parameters, based on the conclusions and equations from previous sections.

A. NOTE ON THE ANTENNA LENGTHS

The gain of the optimal antennas of various lengths (for $\sigma = \sigma_{\text{ref}}$) is shown in Fig. 9 by discrete points. Eq. (5) accurately predicts the gain of antennas whose overall axial length is an

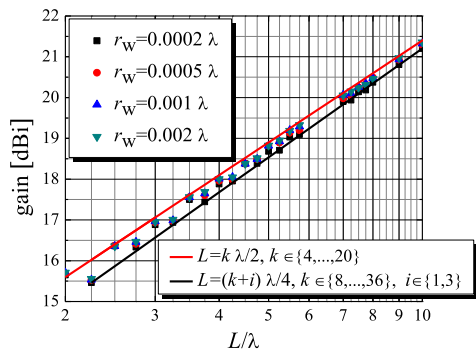


FIGURE 9. Gain for various normalized axial antenna lengths (L/λ) for normalized conductivity $\sigma\lambda = \sigma_{\text{ref}}\lambda$.

integer multiple of half-wavelength, i.e., $L = k\lambda/2$, $k \in \{4, \dots, 20\}$. However, the gain is lower for the optimal antennas for which this condition is not fulfilled. Therefore, in order to achieve the maximal gain, the axial antenna lengths $L = k\lambda/2$, $k \in \{4, \dots, 20\}$ are recommended. In particular, the worst results are observed for the axial antenna lengths $L = (k+i)\lambda/4$, $k \in \{8, \dots, 36\}$, $i \in \{1, 3\}$, when, for shorter antennas, the gain is around 0.4 dB lower than the gain calculated from (5). For longer antennas, the discrepancies are smaller. The red solid line in Fig. 9 fits the gain of the antennas whose axial lengths are $L = k\lambda/2$, $k \in \{4, \dots, 20\}$, whereas the black solid line fits the gain of the antennas whose axial lengths are $L = (k+i)\lambda/4$, $k \in \{8, \dots, 36\}$, $i \in \{1, 3\}$.

B. DESIGN ALGORITHM

The design procedure can be formulated as follows. The targeted antenna gain and wire properties (wire radius and conductivity) are assumed to be known. The normalized axial antenna length can be calculated from (5). This step requires inversion of (5) and numerical calculation. As it is explained in the previous subsection, (5) predicts well the gain of the antennas whose axial length is an integer multiple of half-wavelength. Hence, the normalized axial antenna length calculated from (5) should first be rounded to the nearest greater or equal integer multiple of half-wavelength and then denormalized by multiplication by λ . Next, (6) should be used to check if this design is valid for the desired wire conductor and desired axial antenna length. If the normalized conductivity of the wire conductor is higher than $\sigma_{\text{min}}\lambda$, the design parameters can be calculated from (3), (4). Finally, if it is necessary for a cross-check, the expected gain of the designed antenna can be calculated from (5).

Note that the same design procedure and equations hold for both right-hand and left-hand wound helices.

Since the design equations proposed in the previous section are valid only within a subspace of the hyper rectangle defined in Section I, during the design procedure the practical feasibility of the design should be checked. For example, at 100 MHz all considered axial antenna lengths with all considered wire radii fulfill the limit that

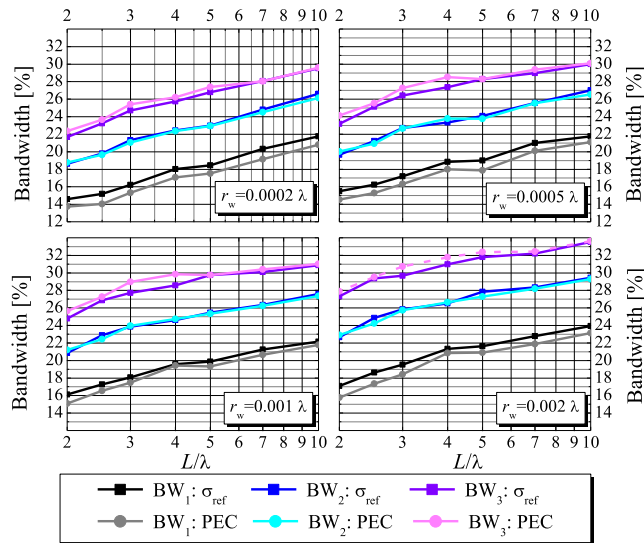


FIGURE 10. Relative bandwidths for the antennas located above an infinite PEC ground plane, versus normalized antenna axial length (L/λ).

the corresponding normalized conductivity $\sigma_{\text{min}}\lambda$ from (6) is lower than 100 MS. However, at 6 GHz the wire radius 0.001λ fulfills the limit for $\sigma_{\text{min}}\lambda$ only for the shortest axial antenna length ($L = 2\lambda$).

Note that if $\sigma_{\text{min}}\lambda$ is too high, the geometrical parameters calculated from (3), (4) can be used as a good starting point for further numerical optimization performed by the designer.

VII. BANDWIDTH, AXIAL RATIO, AND IMPEDANCE OF DESIGNED ANTENNAS

Although the antenna bandwidth and input impedance are not considered within the optimization procedure, they are significant for the applications. Therefore, here we provide values of the bandwidths and input impedances that are inherent to the proposed design. Values of the axial ratios are also presented.

A. RELATIVE BANDWIDTH

We define the relative bandwidth as $\text{BW} [\%] = 100(f_{\text{max}} - f_{\text{min}})/f$, where f_{max} and f_{min} stand for frequencies where the gain is 1 dB (termed as BW_1), 2 dB (BW_2), or 3 dB (BW_3) lower than the maximal gain. Fig. 10 shows the relative bandwidths (BW_1 , BW_2 , and BW_3) for various axial antenna lengths, wire radii, and wire conductivities σ_{ref} from (2), as well as for PEC wires, when the design parameters are calculated from (3), (4) and the antenna is located above an infinite PEC ground plane.

B. AXIAL RATIO AND IMPEDANCE

Fig. 11 shows the axial ratios at the operating frequency in the direction along the antenna axis for various axial antenna lengths and wire radii, when the design parameters are calculated from (3), (4) and the antenna is located above an infinite PEC ground plane. The input impedances of these antennas at the operating frequency are shown in Fig. 12. The axial ratios

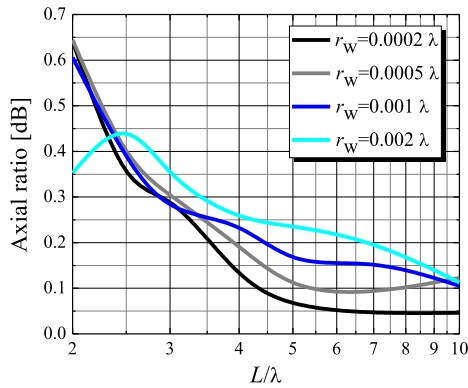


FIGURE 11. Axial ratios of the antennas located above an infinite PEC ground plane, versus normalized antenna axial length (L/λ).

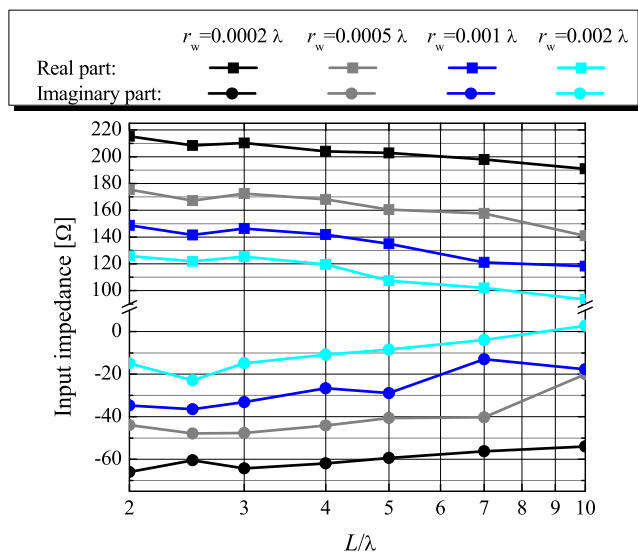


FIGURE 12. Real and imaginary parts of input impedances of antennas located above an infinite PEC ground plane, versus normalized antenna axial length (L/λ), for various wire radii (r_w).

and input impedances at the operating frequency practically do not depend on the wire conductivity.

VIII. FINITE GROUND PLANE

All the previously presented results were obtained for helical antennas located above an infinite PEC ground plane. In practice, the same or even higher gain can be achieved using a square or a circular ground plane of appropriate dimensions.

Fig. 13 shows typical gain differences, Δ gain, between the gain of antennas with a square or a circular plane (of a surface area S) and antennas above an infinite ground plane (calculated from (5)), for various surface areas of the plane and various axial antenna lengths. Differences shown in Fig. 13 are for the reference designs whose wire radius is 0.002λ . For other wire radii, the differences vary less than 0.2 dB compared to the results shown in Fig. 13. The inset of Fig. 13 compares gain differences when the ground plane is a PEC and when its conductivity is σ_{ref} , for the shortest

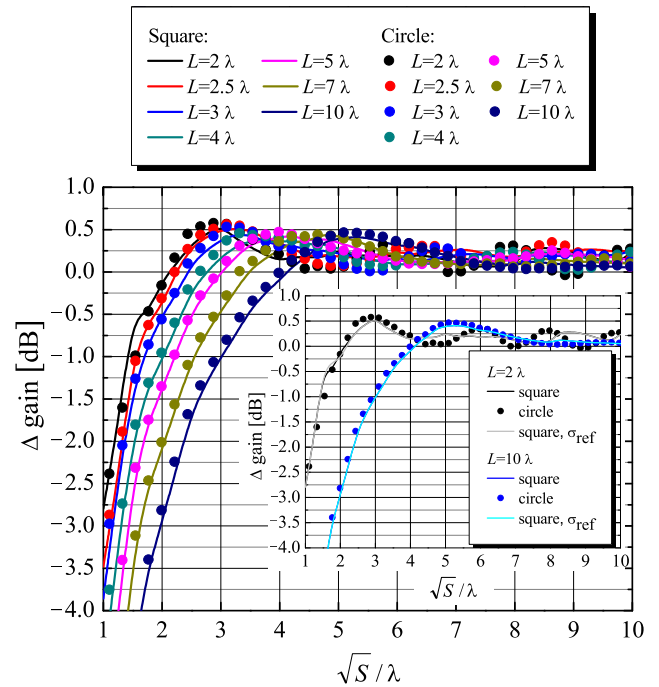


FIGURE 13. Differences between the gain of a helical antenna with a square or a circular ground plane and the gain of the same antenna over an infinite ground plane calculated from (5), versus the normalized square root of the surface area of the plane.

and the longest axial lengths. Results affirm that a circular ground plane is equivalent to a square plane if their surface areas are equal, whereas the effect of losses in the ground plane is negligible.

Further numerical experiments have shown that when the side of the square plane exceeds the dimension sufficient to achieve the maximal gain, the variations of the relative bandwidths are $|\Delta BW_{1,2,3}| < 4\%$, whereas the variations of the axial ratio are less than 0.3 dB. The differences between the input impedances for a square plane, whose side exceeds the value that corresponds to the maximal gain, and for an infinite ground plane are in ranges $-20 \Omega \leq \text{Re}\{\Delta Z\} \leq 60 \Omega$, $-30 \Omega \leq \text{Im}\{\Delta Z\} \leq 10 \Omega$.

IX. DESIGN VERIFICATION

As a worked-out example, we consider a left-hand wound helical antenna. The target gain is 16 dBi, the central operating frequency is 1 GHz (the corresponding free-space wavelength is $\lambda \approx 300$ mm), and the wire parameters are $r_w = 0.6 \text{ mm} \approx 0.002 \lambda$ and $\sigma = 58 \text{ MS/m}$ (copper). The axial antenna length is calculated from (5) and rounded to the first greater integer multiple of the half-wavelength, $L = 2.5 \lambda$. From (6), σ_{min} is calculated to be 7.6 MS/m; hence (3), (4) can be applied to this design. From (3), (4), the design parameters are $r_1 = 0.1051 \lambda$, $r_2 = 0.1453 \lambda$, $\varphi_1 = 4.8438^\circ$, and $\varphi_2 = 5.6121^\circ$. The expected gain, calculated from (5), is 16.40 dBi, which is slightly higher than the targeted gain.

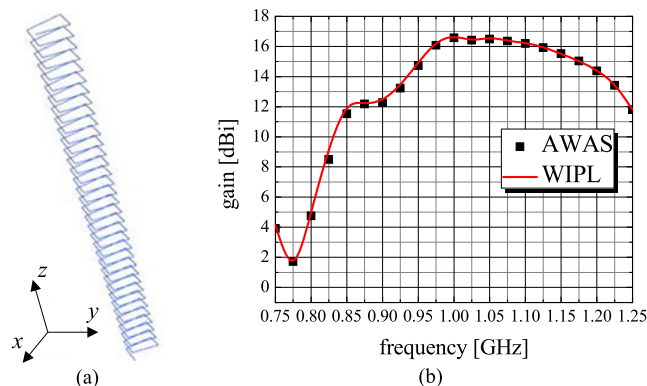


FIGURE 14. (a) WIPL-D model of the antenna designed using calculated parameters and (b) gain of the antenna in a wider frequency range.

A. SIMULATION VERIFICATION

Fig. 14a shows the model of the prototype made using the calculated design parameters, located above an infinite PEC ground plane. The antenna gain calculated by WIPL-D at 1 GHz is 16.62 dBi. Fig. 14b compares the gain in a wider frequency range calculated by WIPL-D and AWAS.

Note that although the design parameters are optimized at a single frequency, the antenna is reasonably broadband. For the antenna shown in Fig. 14a, the relative bandwidths are $BW_1 = 17.98\%$, $BW_2 = 24.61\%$, and $BW_3 = 29.24\%$. The axial ratio at the central operating frequency in the direction along the antenna axis is 0.49 dB. The input impedance at the central operating frequency is $(121.81 - j23.01) \Omega$. The relative bandwidths, axial ratio, and input impedance of the designed antenna agree with the data shown in Figs. 10, 11, and 12, respectively.

In order to produce the prototype, an infinite PEC ground plane was replaced by a finite ground plane. As Fig. 13 indicates, a square ground plane of the side length of 2.25λ is sufficient to achieve the same gain as with the infinite ground plane. Furthermore, with the square ground plane of the side 3.33λ , the gain is 16.93 dBi, which is 0.53 dB higher than the gain calculated from (5), as indicated by Fig. 13. For the designed antenna located above the square ground plane of the side 3.33λ , the relative bandwidths are $BW_1 = 16.84\%$, $BW_2 = 24.53\%$, and $BW_3 = 31.12\%$. The axial ratio at the central operating frequency in the direction along the antenna axis is 0.37 dB and the input impedance at this frequency is $(130.26 - j31.59) \Omega$. The square ground plane of the side 3.33λ is used for the prototype.

A simple technique for matching the antenna to a 50Ω feeder by soldering a properly shaped thin metallic plate is described in [7] and it was implemented here.

B. EXPERIMENTAL VERIFICATION

To experimentally verify our design, we fabricated and measured the antenna introduced as the worked-out example. Acrylic glass was chosen as the material for the supporting structure. This low-cost material has sufficiently low losses

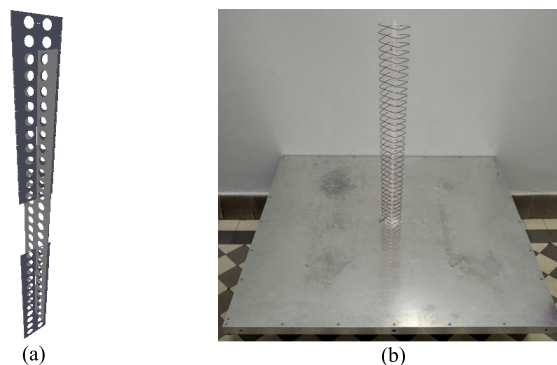


FIGURE 15. (a) Model of the supporting structure and (b) assembled prototype of the antenna.

for the present purpose. The supporting structure consists of acrylic-glass plates tailored and precisely cut in a way to properly intersect and form a cross-like structure. Edges of each plate support corners of the square helix turns. Along the edges of these plates, at appropriate positions, small grooves were cut in order to hold the wire at precise places and thus maintain the calculated pitch angles and turn radii. The model of the supporting structure made in software Blender [39] is shown in Fig. 15a. The supporting structure with wound wire is fixed to an aluminum square plate. The side of the plate is 1 m (i.e., 3.33λ at 1 GHz). The assembled prototype of the antenna is shown in Fig. 15b.

Measurements were performed in the anechoic chamber in Idvorsky laboratories [40]. The gain was measured in the main radiation direction (i.e., in the axial direction), in the frequency range from 750 MHz to 1.25 GHz, and it is compared to the simulations in Fig. 16a. Fig. 16b compares the measured and simulated radiation pattern in the Oxz plane (with respect to the coordinate system shown in Fig. 14a), at the central operating frequency. Due to the imperfect wire bendings at the corners of the turns, the total wire length of the fabricated antenna is around 2.5% longer than in the model. Further, in the model, the antenna conductor is placed in a vacuum, whereas in case of the fabricated antenna the conductor is wound on the dielectric supporting structure, which also slightly affects the antenna properties. Hence, in order to take into account both the effect of imperfect wire bendings at the corners of the turns and the influence of the dielectric, in Fig. 16 we compare measured results with simulated results for the model with the turn radii for 5% larger than the radii calculated from (3). The results shown in Fig. 16 confirm the presented design procedure.

C. COMPARISON WITH OTHER HELICAL ANTENNAS

A detailed investigation and comparison of the uniform helical antennas presented in the literature is given in [7]. As it is shown there, the narrow-band (NB) design achieves the highest gain compared to the other designs presented in the literature, except the gain calculated using the equation from [1], which is considered to overestimate the gain.

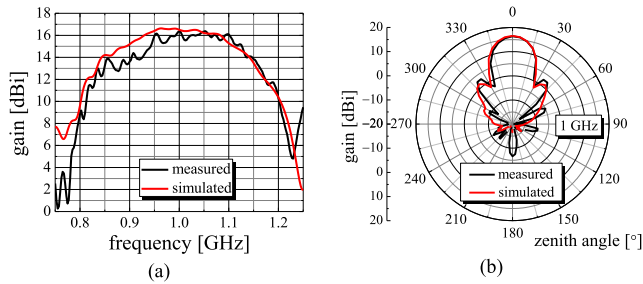


FIGURE 16. Gain of the fabricated antenna (a) in a wider frequency range in the main radiation direction and (b) radiation pattern in Oxz plane at the central operating frequency.

TABLE 2. Comparison of uniform antennas [7] and presented nonuniform antennas for $L = 2 \lambda$.

		$L=2 \lambda$				
		Gain [dBi]	BW ₁ [%]	BW ₂ [%]	BW ₃ [%]	axial ratio [dB]
[7]	σ_{ref}	14.12	20.61	28.46	30.23	1.71
	$1000 \frac{MS}{m}$	14.18	21.45	29.42	31.73	1.72
presented design	σ_{ref}	15.71	16.61	21.73	26.18	0.53
	$1000 \frac{MS}{m}$	16.26	15.5	21.98	26.74	0.54

For these reasons, we believe that the most important comparison of the design presented here is with the NB design from [7].

Tables II–IV compare the gain, bandwidths, and axial ratio of the uniform (NB) antennas from [7] with the nonuniform antennas designed following the presented design procedure at the operating frequency (300 MHz). The results are compared for two different wire conductivities (σ_{ref} and 1000 MS/m). In all cases, the same wire radius ($r_w = 0.0015 \lambda$) is utilized. The nonuniform antennas achieve more than 2 dB higher gain in the case of low losses. The influence of increased losses is smaller on the gain of uniform antennas than on the gain of nonuniform antennas. However, even for higher losses, the nonuniform antennas still achieve a higher gain than the uniform antennas. The bandwidths of the nonuniform helical antennas are wider in case of longer antennas, whereas for shorter antennas the situation is reversed. For all antenna lengths the axial ratio is better in the case of nonuniform helical antennas.

In [9], various types of tapered helical antennas are considered, including the uniform helix. Table V compares the results presented in [9] with the performances of helical antennas designed following the presented design procedure. Since in [9] the radius and conductivity of the helix conductor was not indicated, we utilize $r_w = 0.002 \lambda$ and $\sigma = 58 \text{ MS/m}$ for the antennas designed following the presented design procedure. Instead of the cavity used in [9], we utilize an infinite perfectly conducting ground plane. (Fig. 13 gives information on the influence of the finite ground plane on the gain.)

TABLE 3. Comparison of uniform antennas [7] and presented nonuniform antennas for $L = 4.5 \lambda$.

		$L=4.5 \lambda$				
		Gain [dBi]	BW ₁ [%]	BW ₂ [%]	BW ₃ [%]	axial ratio [dB]
[7]	σ_{ref}	16.61	14.33	17.95	22.22	1.26
	$1000 \frac{MS}{m}$	16.63	14.67	18.73	25.27	1.26
presented design	σ_{ref}	18.38	20.47	26.10	30.40	0.13
	$1000 \frac{MS}{m}$	18.84	20.30	25.90	30.86	0.13

TABLE 4. Comparison of uniform antennas [7] and presented nonuniform antennas for $L = 8.6 \lambda$.

		$L=8.6 \lambda$				
		gain [dBi]	BW ₁ [%]	BW ₂ [%]	BW ₃ [%]	axial ratio [dB]
[7]	σ_{ref}	18.48	11.31	13.46	15.04	1.19
	$1000 \frac{MS}{m}$	18.49	11.35	13.55	15.18	1.19
presented design	σ_{ref}	20.71	23.02	28.05	31.74	0.51
	$1000 \frac{MS}{m}$	21.09	22.68	27.99	31.85	0.50

TABLE 5. Comparison of antennas from [9] and presented nonuniform antennas.

	gain [dBi]		BW ₂ [%]		axial ratio [dB]	
	[9]	*	[9]	*	[9]	*
Uniform 4.46 λ at 900 MHz	16.2	18.4	23	27.5	1	0.3
Tapered-end 4.46 λ at 900 MHz	15.7	18.4	23.8	27.5	0.2	0.3
Continuously tapered 4.8 λ at 1000 MHz	15.8	18.5	31.2	27.3	0.5	1.1
Quasi-tapered 3.84 λ at 800 MHz	14.8	17.8	43.1	24.4	0.5	1.4

*-presented design

From Table V it can be noticed that, for all considered antennas, the gain of the antennas designed following the presented design procedure is for more than 2 dB higher than the gain of the antennas presented in [9]. The goal in [9] was to demonstrate the abilities of nonuniform helical antennas to broaden the bandwidth in comparison with uniform antennas. Hence, the bandwidths of continuously tapered and quasi-tapered helices are wider than the bandwidths of the helices designed following our design procedure, but the gain of our antennas is much higher, as can be expected. The axial ratio in all cases is comparable.

In [12] nonuniformly-wound helical antennas with a wire pigtail counterbalance are reported. The gain of the antennas presented in [12] is compared with the gain of our design, for the axial lengths and wire radii for which our design is applicable. Results of that comparison are listed in Table VI.

TABLE 6. Comparison of antennas from [12] and presented nonuniform antennas.

L/λ	gain [dBi] $r_w=0.001 \lambda$	
	[12]	presented design
2.0	14.03	16.04
2.5	14.68	16.65
3.0	15.55	17.16
3.5	16.10	17.71
4.0	16.44	18.09
4.5	16.83	18.39
5	17.26	18.76

TABLE 7. Comparison of antennas from [15] and presented nonuniform antennas.

		gain [dBi]
$f=2.9 \text{ GHz}, L=2.48 \lambda$	exponential [15]	11.2
	presented design	16.4
$f=2.5 \text{ GHz}, L=2.13 \lambda$	uniform [15]	10.8
	presented design	15.5
$f=2.8 \text{ GHz}, L=3.56 \lambda$	exponential [15]	12.3
	presented design	16.8
$f=2.5 \text{ GHz}, L=3.17 \lambda$	uniform [15]	11.8
	presented design	16.1

For the antennas designed following our design procedure we assumed the wire conductivity to be 58 MS/m and that the antennas are located above an infinite perfectly conducting ground plane. (Fig. 13 gives information about the influence of the finite ground plane on the gain.)

In [15], helical antennas with exponentially varying spacing between the turns are presented and compared with the uniform helical antennas. Table VII compares the presented design with the designs from [15] for the same axial antenna length, wire conductivity, ground plane shape, and dimensions. For antennas designed by our procedure the wire radius is 0.002λ .

The gain of the antennas designed following the presented design procedure is for more than 4.5 dB higher than the gain of the antennas from [15].

Further, in [41] the design of a uniform helical antenna at 5.25 GHz is presented. The simulated gain is 12.58 dBi. For the same axial length and conductor radius, the gain of the nonuniform helical antenna designed following our procedure is 16.2 dBi if the antenna is located above a ground plane of appropriate dimensions.

X. CONCLUSION

The paper presents a rapid and reliable procedure for the design of nonuniform helical antennas with linearly varying geometrical parameters. Using numerical optimization, we made a large database of the optimal antennas. Based on these results, we proposed analytical equations for the design of antennas with desired characteristics, which require only a few simple steps. Properties of antennas designed using

the present design equations were discussed. This design procedure was verified by simulations and experiments.

The large database formed throughout the research presented in this paper can be further utilized to train machine learning algorithms, for the design of nonuniform helical antennas. This investigation will be the scope of our future work.

ACKNOWLEDGMENT

The views and findings in this paper are those of the authors and do not reflect the views of DARPA.

REFERENCES

- [1] J. D. Kraus, "Helical beam antennas," *Electronics*, vol. 20, pp. 109–111, Apr. 1947.
- [2] J. D. Kraus, "The helical antenna," in *Antennas*, 2nd ed. New York, NY, USA: McGraw-Hill, 1988, ch. 7, pp. 265–339.
- [3] G. A. Thiele and W. L. Stutzman, "Helical antennas," in *Antenna Theory and Design*, 3rd ed. New York, NY, USA: Wiley, 2012, ch. 7, pp. 225–233.
- [4] H. King and J. Wong, "Characteristics of 1 to 8 wavelength uniform helical antennas," *IEEE Trans. Antennas Propag.*, vol. AP-28, no. 2, pp. 291–296, Mar. 1980.
- [5] J. L. Wong and H. E. King, "Empirical helix antenna design," in *Proc. Antennas Propag. Soc. Int. Symp.*, vol. 20, May 1982, pp. 366–369.
- [6] D. T. Emerson, "The gain of the axial-mode helix antenna," *Antenna Compendium*, vol. 4, pp. 64–68, Mar. 1995.
- [7] A. R. Djordjevic, A. G. Zajic, M. M. Ilic, and G. L. Stuber, "Optimization of helical antennas [antenna Designer's notebook]," *IEEE Antennas Propag. Mag.*, vol. 48, no. 6, pp. 107–115, Dec. 2006.
- [8] D. J. Angelakos and D. Kajfez, "Modifications on the axial-mode helical antenna," *Proc. IEEE*, vol. 55, no. 4, pp. 558–559, Apr. 1967.
- [9] J. Wong and H. King, "Broadband quasi-taper helical antennas," *IEEE Trans. Antennas Propag.*, vol. AP-27, no. 1, pp. 72–78, Jan. 1979.
- [10] H. M. Elkamchouchi and A. I. Salem, "Helical antennas with nonuniform helix diameter," in *Proc. 18th Nat. Radio Sci. Conf.*, Mar. 2001, pp. 143–152.
- [11] H. M. Elkamchouchi and A. I. Salem, "Effects of geometrical parameters, loading, and feeding on nonuniform helical antennas," in *Proc. 19th Nat. Radio Sci. Conf.*, Mar. 2002, pp. 90–100.
- [12] R. Golubovic, A. Djordjevic, D. Olcan, and J. Mosig, "Nonuniformly-wound helical antennas," in *Proc. 3rd Eur. Conf. Antennas Propag.*, Berlin, Germany, Mar. 2009, pp. 3077–3080.
- [13] A. M. Menon and S. S. Kumar, "Optimum design of axial mode helical antenna with nonlinear pitch profile modeled using Catmull-Rom spline and Particle Swarm Optimization," in *Proc. Int. Conf. Commun. Signal Process.*, vol. 1, Feb. 2011, pp. 146–150.
- [14] K. Jimisha and S. Kumar, "Optimum design of exponentially varying helical antenna with non uniform pitch profile," *Procedia Technol.*, vol. 6, pp. 792–798, Jan. 2012.
- [15] C.-H. Chen, E. K. N. Yung, B.-J. Hu, and S.-L. Xie, "Axial mode helix antenna with exponential spacing," *Microw. Opt. Technol. Lett.*, vol. 49, no. 7, pp. 1525–1530, Jul. 2007.
- [16] I. Egorov and Y. Zhinong, "A non-uniform helical antenna for dual-band cellular phones," in *Proc. IEEE Antennas Propag. Soc. Int. Symp.*, vol. 2, Jul. 2000, pp. 652–655.
- [17] G. Zhou, "A non-uniform pitch dual band helix antenna," in *Proc. IEEE Antennas Propag. Soc. Int. Symp.*, Jul. 2000, pp. 274–277.
- [18] J. Dinkić, D. Olčan, and A. Djordjević, "Comparison of various geometries of nonuniform helical antennas," in *Proc. 6th Int. Conf. Elect., Electron. Comput. Eng. (ICETAN)*, Srebrno Jezero, Serbia, 2019.
- [19] S. J. Mazlouman, A. Mahanfar, C. Menon, and R. G. Vaughan, "Reconfigurable axial-mode helix antennas using shape memory alloys," *IEEE Trans. Antennas Propag.*, vol. 59, no. 4, pp. 1070–1077, Apr. 2011.
- [20] X. Liu, S. Yao, S. V. Georgakopoulos, B. S. Cook, and M. M. Tentzeris, "Reconfigurable helical antenna based on an origami structure for wireless communication system," in *IEEE MTT-S Int. Microw. Symp. Dig.*, vol. 1, Jun. 2014, pp. 1–4.

- [21] W. Su, R. Bahr, S. A. Nauroze, and M. M. Tentzeris, "3D printed reconfigurable helical antenna based on microfluidics and liquid metal alloy," in *Proc. IEEE Int. Symp. Antennas Propag.*, Fajardo, Puerto Rico, Jun./Jul. 2016, pp. 469–470.
- [22] S. Yao and S. V. Georgakopoulos, "Origami segmented helical antenna with switchable sense of polarization," *IEEE Access*, vol. 6, pp. 4528–4536, Dec. 2017.
- [23] S. I. H. Shah, S. Ghosh, and S. Lim, "A novel DNA inspired mode and frequency reconfigurable origami helical antenna," in *Proc. IEEE Int. Symp. Antennas Propag. USNC/URSI Nat. Radio Sci. Meeting*, Boston, MA, USA, Jul. 2018, pp. 187–188.
- [24] S. Singh, J. Taylor, H. Zhou, A. Pal, A. Mehta, H. Nakano, and P. Howland, "A pattern and polarization reconfigurable liquid metal helical antenna," in *Proc. IEEE Int. Symp. Antennas Propag. USNC/URSI Nat. Radio Sci. Meeting*, Boston, MA, USA, Jul. 2018, pp. 857–858.
- [25] X. Liu, C. L. Zekios, and S. V. Georgakopoulos, "Analysis of a packable and tunable origami multi-radii helical antenna," *IEEE Access*, vol. 7, pp. 13003–13014, 2019.
- [26] A. R. Djordjevic, M. M. Ilic, A. G. Zajic, D. I. Olcan, and M. M. Nikolic, "Why does reflector enhance the gain of helical antennas?" in *Proc. 2nd Eur. Conf. Antennas Propag.*, Edinburgh, U.K., Nov. 2007, pp. 1–8.
- [27] A. R. Djordjevic, A. G. Zajic, and M. M. Ilic, "Enhancing the gain of helical antennas by shaping the ground conductor," *IEEE Antennas Wireless Propag. Lett.*, vol. 5, no. 1, pp. 138–140, Dec. 2006.
- [28] D. I. Olcan, A. G. Zajic, M. M. Ilic, and A. R. Djordjevic, "On the optimal dimensions of helical antenna with truncated-cone reflector," in *Proc. 1st Eur. Conf. Antennas Propag.*, Nice, France, Nov. 2006, pp. 1–6.
- [29] F. Sadeghnia, M. Mahmoodi, H. Hashemi-Meneh, and J. Ghayoomeh, "Helical antenna over different ground planes," in *Proc. 8th Eur. Conf. Antennas Propag.*, The Hague, Netherlands, Apr. 2014, pp. 2185–2188.
- [30] J. Dinkić, M. Tasić, and A. R. Djordjević, "Influence of conductor shape and size on properties of helical antennas," in *Proc. 5th Int. Conf. Elect., Electron. Comput. Eng. (IcETRAN)*, Palić, Serbia, 2018, pp. 605–608.
- [31] WIPL-D. (2017). *WIPL-D Pro v11.0-3D EM Solver*. Belgrade, Serbia. [Online]. Available: <https://www.wipl-d.com>
- [32] A. R. Djordjević, M. B. Baždar, V. V. Petrović, D. I. Olćan, T. K. Sarkar, R. F. Harrington, "AWAS for windows: Analysis of wire antennas and scatterers," in *Software and User's Manual*, Boston MA, USA: Artech House, 2002.
- [33] *IEEE Standard Definitions of Terms for Antennas*, IEEE Standard 145-1983, 1983.
- [34] J. Dinkić, D. Olćan, A. Djordjević, and A. Zajić, "Comparison of optimization approaches for designing nonuniform helical antennas," in *Proc. IEEE Int. Symp. Antennas Propag. USNC/URSI Nat. Radio Sci. Meeting*, Boston, MA, USA, Jul. 2018, pp. 1581–1582.
- [35] J. Kennedy and R. Eberhart, "The particle swarm," in *Swarm Intelligence*, 1st ed. San Mateo, CA, USA: Morgan Kaufmann, 2001, ch. 7, pp. 287–326.
- [36] J. Robinson and Y. Rahmat-Samii, "Particle swarm optimization in electromagnetics," *IEEE Trans. Antennas Propag.*, vol. 52, no. 2, pp. 397–407, Feb. 2004.
- [37] J. A. Nelder and R. Mead, "A simplex method for function minimization," *Comput. J.*, vol. 7, no. 4, pp. 308–313, 1965.
- [38] B. D. Popovic, "Electromagnetic field theorems," *IEE Proc. A-Phys. Sci., Meas. Instrum., Manage. Educ.-Rev.*, vol. 128, no. 1, pp. 47–63, Mar. 1981.
- [39] *Blender—A 3D Modeling and Rendering Package*, Blender Found., Amsterdam, The Netherlands, 2017.
- [40] *Idvorsky Laboratories*. Accessed: Sep. 1, 2019. [Online]. Available: <http://www.idvorsky.com/en/>
- [41] M. Márton, L. Ovseník, J. Turán, M. Špes, and J. Vásárhelyi, "Possibility of increasing availability of FSO/RF hybrid system with implementation of helix antenna for 5.2GHz," in *Proc. 19th Int. Carpathian Control Conf.*, May 2018, pp. 498–501.

• • •